Title: Implantable Bioelectronics for Real-time *in vivo* Recordings of Enteric Neural Activity

Authors: Alexander J. Boys[1,2]†, Amparo Güemes[3]†, Rohit A. Gupta[4], Friederike H. Uhlig[5,6], Niall P. Hyland[5,6], David C. Bulmer[4], George G. Malliaras[3]*, Róisín M. Owens[1]*

Affiliations:

[1]Department of Chemical Engineering & Biotechnology, University of Cambridge; Cambridge, UK

[2]Thayer School of Engineering, Dartmouth College; Hanover, NH, USA

[3]Department of Engineering, University of Cambridge; Cambridge, UK

[4]Department of Pharmacology, University of Cambridge; Cambridge, UK

[5]Department of Physiology, University College Cork; Cork, Ireland

[6]APC Microbiome Ireland, University College Cork; Cork, Ireland

†These authors contributed equally to this work.

*Co-corresponding authors. Email: gm603@cam.ac.uk & rmo37@cam.ac.uk

Abstract: The enteric nervous system represents a primary point of contact for a host of factors that influence bodily health and behavior. This division of the autonomic nervous system is unique in both its extensivity, with neurons distributed throughout the gastrointestinal tract from the esophagus to the rectum, and its capability for local information processing. Here, we show the construction and validation of a bioelectronic device to access neural information produced and processed in the gastrointestinal tract. We designed an implant and concurrent surgical procedure to place a neural recording device within the wall of the colon of rodents. We captured complex multi-frequency electrophysiological responses to neural stimulants and show that we can record activity in the context of mechanical activity mimicking gut motility. We also show the feasibility of utilizing this device for recording colonic activity in freely-moving animals. This work represents a step forward in devising functional bioelectronic devices for understanding the complex pathways of the gut-brain axis.

One-Sentence Summary: Bioelectronic device for real-time collection of neural information from the enteric nervous system.

Main Text: The enteric nervous system (ENS) is an expansive network of neurons and supporting cells that drives gut physiology. This system plays a major role in controlling gut motility, ion and mucus secretion, and vasodilation (*1*, *2*) and is an essential part of the bidirectional gut-brain axis, affecting health and behavior (*3*, *4*). Unlike other areas of the peripheral nervous system, the ENS is also capable of processing local information through individualized neural circuits that act independently of the central nervous system (*1*). Recent work has focused on physiological and biochemical outputs, which has resulted in the discovery of significant bidirectional connections between activity in the ENS and behavioral and pathologic changes elsewhere in the body (*4–6*), making exploration of the ENS timely.

The ENS consists of two interconnected ganglionated plexi (myenteric and submucosal) that wrap circumferentially around the gastrointestinal (GI) tract (*1*). Given their positioning in the gut, these plexi are difficult to access, making monitoring of neural signaling within the ENS challenging. Adding difficulty is the relative inaction of the ENS under general anaesthesia (*7*), which results in limited and/or low-amplitude local signaling. These challenges necessitate the construction of a neural recording device that can achieve close proximity to the ENS with a low impedance to maximize signal transduction across the device interface. Traditional neural recording devices are not compatible with the constant intrinsic and extrinsic motion of the gut and fail to maintain conformal contact within the context of the highly contoured and elastic tissue that constitutes the GI tract. As such, past studies have primarily utilized standard electrophysiological techniques that are not suitable for *in vivo* implantation and have focused instead on *ex vivo* recordings using organ baths, patched electrophysiological setups, and / or calcium and voltage imaging (*8–11*). Recent advances in the development of flexible neural probes have allowed for the construction of flexible bioelectronic devices that are compatible with soft tissues and are capable of maintaining a sustained electrical interface with local neural populations (*12–14*). Even with these advancements, only one study to-date to the best of our knowledge, has been able to access the gut using *in vivo* implantable technologies (*15*), and this study was not directed at monitoring electrophysiological neural action.

Here, we develop a custom bioelectronic implant system for conducting *in vivo* neural recordings within the colonic wall of rodents. First, we record neural responses of local gut electrophysiology elicited through the use pharmacological neural stimulants in anaesthetized rodents. We then show that changes in electrical activity can be recorded in response to distension of the gut. Finally, we developed a secondary set of implants with integrated backend electronics and an associated surgical technique for performing recordings in freely-moving animals, showing changes in response during nutritional intake. This study opens up the potential to monitor ENS activity continuously in real time along the length of the GI tract, to not only increase our fundamental understanding of the ENS and GI physiology, but also to understand the gut-brain axis' influence on behavior.

Implant Design & Surgery Development

We designed an implantable bioelectronic device for recording neural signals from the ENS *in vivo* (Fig. 1A). The devices are based on state-of-the-art bioelectronic device fabrication principles, utilizing a flexible, dielectric substrate for tissue contact and a series of open neural recording electrodes coated with the conducting polymer, poly(ethylene dioxythiophene):poly(styrene sulfonate) (PEDOT:PSS), reducing impedance and therefore electrode size for improved neural recording capabilities (*16*). The devices were produced using photolithographic microfabrication techniques (*13*, *17*) using a parylene-C substrate and

insulator, gold tracks, and gold electrodes coated with PEDOT:PSS. We designed the device with the required size specifications to reside within the walls of the colon and provide enough spatial resolution based on the neuronal clusters (plexi) observed in the ENS (*1*). We additionally included a series of markers and loops to assist in the surgical placement of the device in juxtaposition with the ENS (Fig. S1).

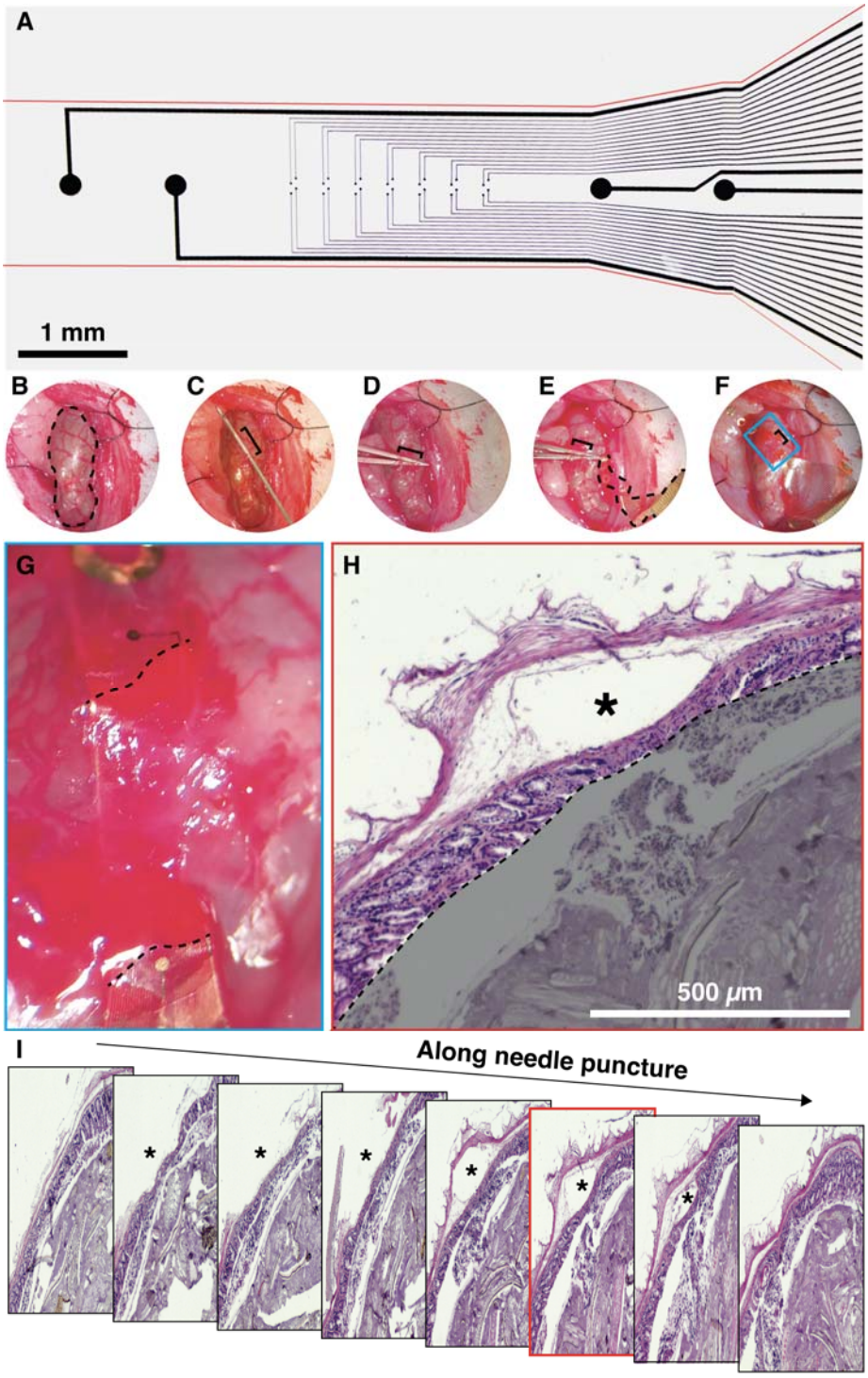

Fig. 1. Implant design and surgical placement. (**A**) Brightfield image taken in transmission showing the device layout for accessing the ENS. Devices consist of gold tracks insulated with parylene-C with PEDOT:PSS-coated gold electrodes, containing a linear array of 7 sets of 4 electrodes, each 20 μm in diameter, flanked on either side by a pair of large electrodes, 200 μm in size, which were used as surgical markers. Given that the device substrate (parylene-C) is translucent, the outline of the device has been highlighted in red. (**B** to **F**) Steps for implanting device into the colonic wall, shown via stereoscope during surgery. Dotted line in (**B**) indicates the periphery of the section of colon under analysis. Brackets in (**C**) indicate the section of needle that is situated in the wall of the colon. Brackets in (**D**) and (**E**) indicate the section of forceps that are within the wall. Dotted line in (**E**) highlights the outer edges of the implant. Bracket in (**F**) shows the section of implant that is in the colonic wall. Inset from (**F**) in blue box is shown in (**G**) with device situated beneath the muscularis externa. Dotted lines indicate where the device enters (bottom dotted line) and exits (top dotted line) the tissue. One of the 200 μm electrodes is visible just past the dotted line where the device exits the tissue. At the top edge of the image, a loop which is used to assist in placement of the device, is also visible. (**H**) Hematoxylin and eosin histological stain of needle placement in colonic wall, which is used to create the tunnel for the implant as shown in (**C**). This image shows that this implantation technique results in placement directly below the muscularis externa. Asterisk indicates the tunnel in the tissue where the needle was threaded through the colonic wall. The lumen of the gut, which contains fecal matter is shaded in gray. (**I**) Axial series of hematoxylin and eosin histological images showing the progression of the needle along the colon with the tunnel in tissue indicated via asterisks. Image in (**H**) is shown with a red border in (**I**) in sequence with other images. Brightness and contrast have been adjusted on images to highlight features.

To access the ENS, we did a laparotomy and isolated the colon from the surrounding tissue (Fig. 1B). To place the device, we ran a needle underneath the muscularis externa of the colon (Fig. 1C) and then back-tracked along this tunnel using a pair of reverse-action forceps (Fig. 1D). We then located and gripped the leading edge of the implant (Fig. 1E) and threaded the implant through the tunnel with the electrodes facing luminally to record from the submucosal plexus (Fig. 1F and G). As we situated the recording electrodes of the device in the center of the dielectric substrate, we could thus ensure some level of insulation from high frequency signals originating in the myenteric plexus. The placement of the implant within the wall of the colon also facilitates tight contact with surrounding tissues, even during acute recordings, due to tissue elasticity, which limits the effect of blood, other accumulating fluids, and breathing on the quality of the electrophysiological recordings (Movies S1 and S2). To confirm appropriate placement of the implant, we performed histology on the location where the needle was threaded into the colonic wall, identifying the positioning of the tunnel as luminally adjacent to the muscularis externa (Fig. 1H). Tracking the axis of the tunnel (Fig. 1C) histologically (Fig. 1I), we show that we can place these needles without puncturing through the submucosal and mucosal layers into the lumen.

Confirmation of Recording Capabilities from the ENS through Drug Administration

After developing the device and associated surgery, we conducted an assessment of the recording capabilities of our devices by capturing elicited compound activity in response to sensory neural stimulants (Fig. 2 and S2). To confirm drug dosing concentrations, we recorded responses to the prototypic noxious inflammatory stimuli, bradykinin - an established chemical nociceptive stimuli relevant to tissue injury and pain via G-protein-coupled receptors (*18*), and capsaicin -

the active ingredient in peppers which acts on transient receptor potential vanilloid type 1 (TRPV1) channels in nociceptive sensory neurons (*19*), consistent with colonic afferent responses to these mediators seen in *ex vivo* recordings of lumbar splanchnic nerve (LSN) bundles from the mouse colon (Fig. S3).

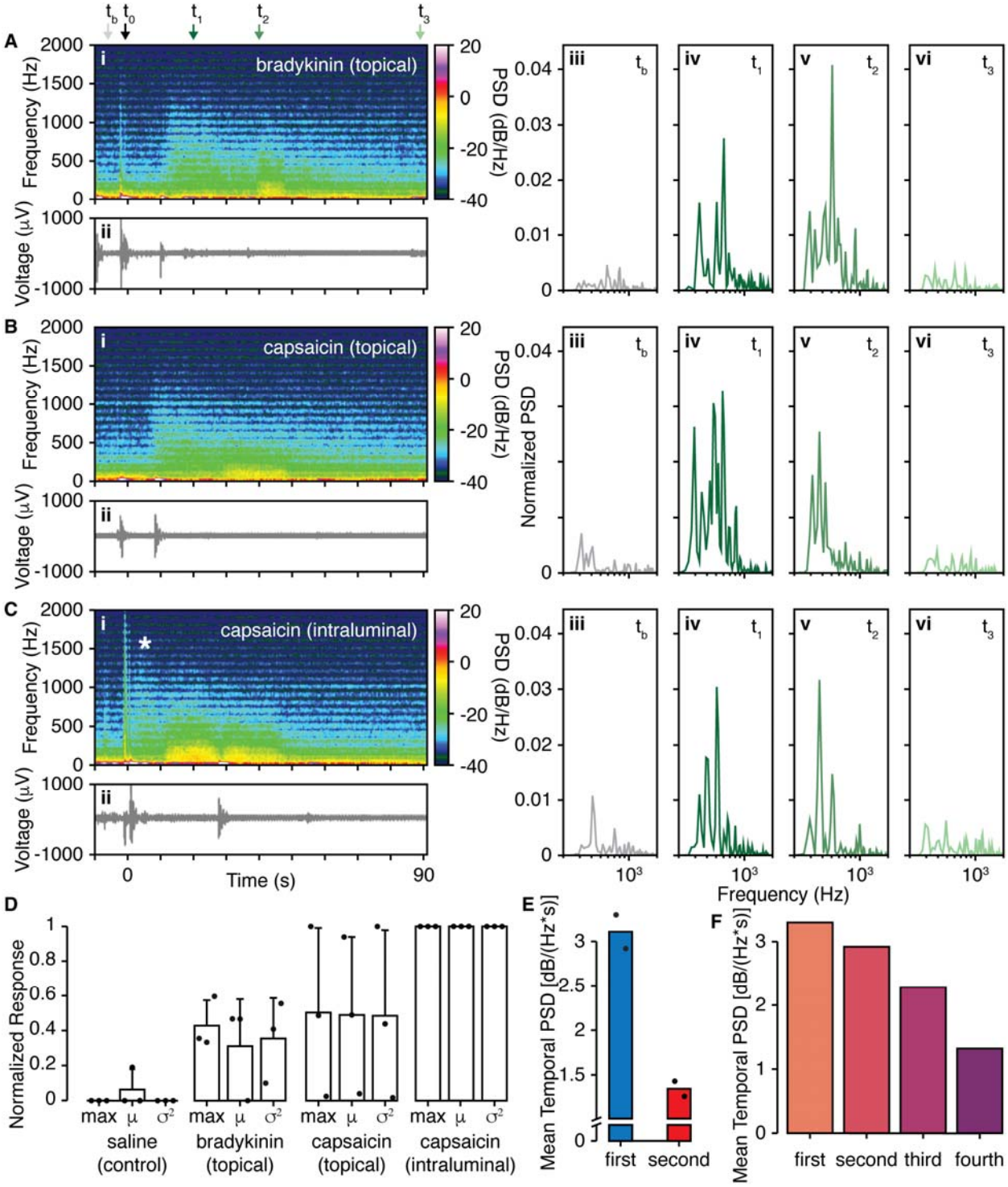

Fig. 2. Pharmacological stimulation of the ENS. Representative responses to (**A**) topical administration of 10 μM bradykinin, (**B**) topical administration of 500 nM capsaicin, and (**C**)

intraluminal administration of 500 nM capsaicin, showing (**i**) spectrogram (0 - 2000 Hz) of power spectral density (PSD), (**ii**) raw voltage signal, and normalized power spectra (zoom in 200 - 1400 Hz) at (**iii**) t_0, (**iv**) t_1, (**v**) t_2, and (**vi**) t_3, time points semi-arbitrarily chosen to highlight change in the relative power spectra across the recording and indicated in (**A**) with color-coded, labeled arrows. Drug administration occurred at approximately t_0 for (**A**), (**B**), and (**C**). Asterisk in (**C**) indicates initial high frequency response as discussed in the text. (**D**) Normalized response to different drug additions (n = 3 rats). The response activity elicited by each drug was quantified with the maximum [dB/(Hz*s)], mean [dB/(Hz*s)], and variance {[dB/(Hz*s)]^2} of the temporal power spectral density (PSD), computed as the area under the curve (AUC) of the spectrogram power data using non-overlapping 1 s rolling windows. The responses were normalized [0,1] to the maximum and minimum values obtained among all additions (including saline) to allow for meaningful comparisons. (**E**) Mean of the temporal PSD (200 - 3000 Hz) for an initial and secondary administration of bradykinin (repeated twice) with no intermediate saline wash for a rat. (**F**) Mean of the temporal PSD (200 - 3000 Hz) for 4 consecutive additions of bradykinin with wash steps in between.

We utilized these data to design an *in vivo* experiment using our colonically-placed bioelectronic devices to record the electrophysiological response to dropwise topical addition of 10 µM bradykinin (Fig. 2A) and 500 nM capsaicin to the serosal side (topically) of the GI tract (Fig. 2B), and intraluminal injection of 500 nM capsaicin (Fig. 2C), achieved by placing a needle into the colon in the vicinity of the implant and delivering the solution into the luminal cavity using a syringe pump. These additions were performed in this sequence to account for the known desensitizing properties of capsaicin (*20*). Each administration was followed by multiple washes with saline, which also provides an intermediate non-pharmacological comparative signal showing no response (Fig. S4), and a waiting period of at least 5 minutes to reduce cross-effects from different drugs.

The topical application of bradykinin occurred at t_0, defined as 0 s, followed by approximately 10 s of inactivity, proceeding to 60 s of sustained activity at and below 1500 Hz (Fig. 2Ai), with large low-frequency contributions visible in the raw voltage trace (Fig. 2Aii). The baseline in the power spectrum (Fig. 2Aiii), taken prior to drug addition, was followed by the presence of substantial and varying high-frequency contributions below 1000 Hz during the sustained portions of the response (Fig. 2Aiv and v) before dropping back to the baseline at the end of the response (Fig. 2Avi).

The response to topical addition of capsaicin showed similar onset of response to the topical bradykinin with an approximate 10 s delay after drug addition before the development of a sustained response (Figs. 2B). This delay can be attributed to the absorption time required for the drug to permeate the tissue. Similar to the bradykinin, an increase in low frequency power is visible approximately 30 s after the initial drug addition, before reverting to baseline (Fig. 2Bvi). While this portion of the response also contains high frequency components, these aspects are shifted to lower frequencies below 500 Hz (Fig. 2Bv). The initial transient high-frequency response is possibly linked to afferent sensory activation in the myenteric plexus, which then triggers the transmission of electrical signals between electrically coupled muscle cells through gap junctions, resulting in sustained lower-frequency activity.

Intraluminal injection of capsaicin shows a different response, with an increase in the signal power relative to topical addition of capsaicin at the same concentration. While a 10 s delay is visible before the sustained response, this intermittent period also contains signal across

numerous frequencies up to 1500 Hz (Fig. 2C, marked with an asterisk), probably due to the stimulation of stretch receptors in the myenteric plexus and / or muscularis externa (*21*), together with the activation of TRPV1 receptor on submucosal neuroendocrine cells from the luminal side (*22*). This activation could then lead to a complex response including the release of hormones such as serotonin that subsequently activate the ENS, illustrated by a substantial surge in power below 500 Hz with some high frequency contributions (Figs. 2Ci, iv and v), until returning to baseline values approximately 60 s after injection (Fig. 2Cvi).

These results were quantified by normalized metrics extracted from the temporal power spectral density (Fig. 2D) and compared to a saline addition (Fig. S4, used as a control). The results from the bradykinin addition show a relatively consistent increase in signal, whereas the topical capsaicin addition is somewhat inconsistent in its response magnitude across multiple experiments. The intraluminal capsaicin injection results in a consistently substantial response, as expected. However, the positioning of the device in the colon wall with respect to the sparse distribution of neurons and other electrophysiologically-active cells, makes exact placement of an implant in these positions very difficult. Further work in generating a mapping mechanism, similar to the concept of the stereotaxic frame for brain surgery, would greatly aid efforts towards deconvoluting single cell electrophysiology and similar from the complex spectrograms that we record in these scenarios.

The raw voltage waveforms for all drugs are dominated by large, low frequency signals visible in white at the lowest frequencies of the spectrogram (Fig. 2Ai, Bi, and Ci) and in the corresponding voltage waveform (Fig. 2Aii, Bii, and Cii). These low frequency characteristics do not illustrate the full spectral response that is observed after drug addition and are likely associated with mechanical artifacts from tissue motion during drug addition or needle placement, micro-contractions (i.e. low frequency contractions not differentiable from breathing by eye), and / or distension of the colonic wall during injection in the case of intraluminal capsaicin, depending on the temporal location of the low frequency signal. Responses for capsaicin and bradykinin (Figs. 2A, B, and C) should all be considered in the context of a saline addition as a control (Fig. S4), where no spectral changes are observable after the initial addition of saline, and the response metrics register the minimum (Fig. 2D).

To examine whether the bradykinin-induced response is reduced as a consequence of receptor desensitization (*23*), we performed multiple doses in one animal. The addition of bradykinin followed by a second addition of bradykinin with no intermediate wash, repeated twice (Fig. 2E), shows a reduction in signal power density on the second dose. Then, two more subsequent additions of bradykinin (3rd, and 4th), all occurring after the first set and separated by washes (Fig. 2F), each show a reduction in power density per dose.

Considering spatial and frequency dynamics, our extracellular electrodes allow us to capture signals from the numerous sources that collectively contribute to the recorded electrophysiological activity of the colon, including sensory and motor neurons, neuroendocrine cells, smooth muscle depolarization, and ENS activity. The multifaceted nature of these signals underscores the complexity of neural interactions within the network. Using our device in this context, we can also reduce some aspects of the signal contribution from sources of high electrical activity through positioning of the insulating portions of the implant towards a source. In this case, we placed the insulating backing towards the muscularis externa to reduce contributions from the myenteric plexus, thereby also facing the electrodes towards the submucosal plexus of the ENS. When evaluating the resultant signal in all cases, we observe

distinct patterns of activation observed with different routes of drug administration, indicating the presence of various mechanisms of action, each exhibiting unique dynamics especially in the high-frequency components of the signals. These observations, in the context of our use of sensory neural stimulants, e.g. bradykinin and capsaicin, indicate our capability for recording neural signals related to the ENS.

Recording During Colonic Contraction

As noted above, gut motility is inhibited during general anaesthesia (*7*), which has traditionally made acute neural recordings in the ENS a challenge. While our device was able to receive signal from the ENS in response to addition of neural stimulants, large-scale gut motility was largely absent. However, as proof of the capability of our device to measure colonic contraction, in one instance we recorded activity during a substantial colonic contraction (Fig. 3), spontaneously initiated after saline addition to the colon while the animal was anaesthetized. This contraction was observed as a ~10 mm, multiaxial rostral movement followed by a caudal relaxation back to its initial conformation (Fig. 3A). The spectrogram trace of the contraction differs significantly from those observed during drug administration with a signal that monotonically decreases in power from high to low frequency both at any point in time and temporally throughout the contraction (Fig. 3B). Given that our bioelectronic device possesses multiple electrodes positioned at discrete locations along the colon, we can also spatially examine this contraction as a function of distance along the colon. Given the unique nature of this contraction in the context of the other experiments we performed in this study, we could not determine the spatial origin of the contraction, however, we recorded differences in voltage magnitude at multiple locations in the colon, noting variations in the response waveform dependent on location (Fig. 3C). Finally, the envelope of the high frequency bandpass filtered voltage signals (300 to 2000 Hz) recorded from each electrode allowed us to visualize the signal amplitude's progression during the contraction. The average envelope for the waveform of this contraction (Fig. 3D) shows an initial peak occurring at approximately 50 s from the beginning of the trace, followed by a shoulder lasting from around 60 to 100 s, before decreasing to baseline.

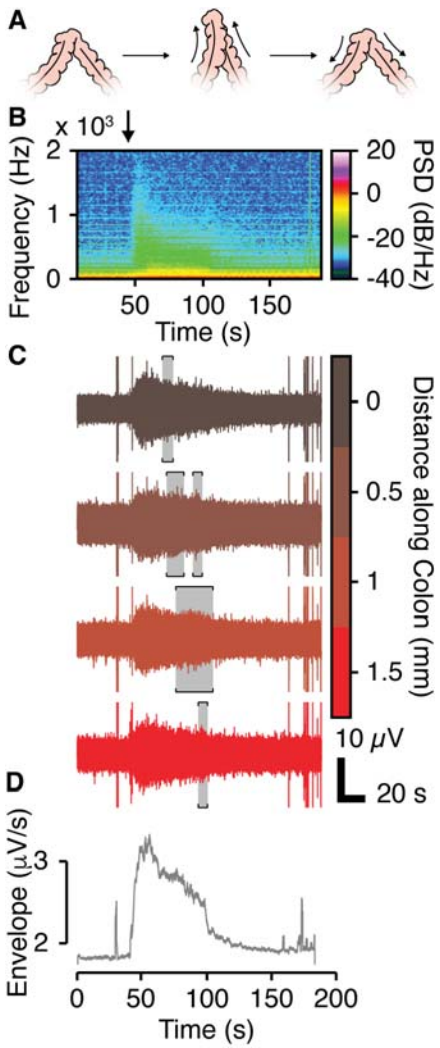

Fig. 3. Recording of Colonic Contraction. (**A**) Schematic showing the approximate contractile conformation that was observed. (**B**) Spectrogram of the raw data for the contraction trace (n = 1 rat). Thick black arrow indicates the approximate beginning of the contraction. (**C**) High-frequency bandpass voltage traces (300 to 2000 Hz) from multiple electrodes positioned along the colon during the contraction. Differences in the envelope (i.e. shape) are observed at different locations. Variations between these traces are highlighted in each response using shaded brackets. (**D**) Average voltage envelope for all electrodes during contraction calculated using the Hilbert transform method followed by a 1 s rolling window smoothing procedure. This waveform is indicative of the general shape across the entire recording region of the colon. All traces are scaled to the same y-axis. Sharp signal prior to the arrow in (**B**) is the saline addition.

Response to Mechanical Stimuli

Following the assessment of the device's capability to record responses to nociceptive stimuli induced by drugs and the observation of its ability to capture spontaneous contractions, we examined the ability of the device to record spontaneous compound activity originating from mechanical distensions of the gut wall. This interest is driven by the finding that gut distension, which occurs during gut motility, is associated with neural action, both in driving peristalsis of the gut and in the context of stretch-sensitive neurons that activate during distension of the tissue

(*24*). To examine this phenomenon, we performed saline distensions of ligated portions of the colon during electrophysiological recording (Fig. 4, Movie S3). To distend the colon, we placed sutures around the adjacent portions of the colon prior to implantation and ligated the colon to fluidically isolate approximately 1 cm of colon, where we implanted the device as described before (Fig. 1B to G). After implantation, we placed a needle into the colon in the vicinity of the implant (Fig. 4A) and injected ~0.3 mL of saline into the colon using a syringe pump, thereby distending the tissue (Fig. 4B, Movie S3), while recording the evoked electrical activity. The extent and duration of the distension primarily relied on the level of ligation, carefully performed to close the lumen without causing tissue damage.

Using this setup, we examined the tissue response to mechanical distension at both high frequency (300 - 2000 Hz) and low frequency (0 - 300 Hz) (Fig. 4C). We performed two distensions under low isoflurane (1.3%) (Fig. 4C, blue traces). We increased the isoflurane content (5%) (Fig. 4C, dotted line), and performed two further distensions (Fig. 4C, red traces). We allowed time between each event for the tissue and related activity to recover (Fig. 4C). By extracting 10 s windows of voltage traces after each distension, we observe an initial fast peak in the high-frequency trace (Fig. 4D, blue traces), followed by an extended voltage response, visible in the low-frequency trace (Fig. 4E, blue traces) before returning to baseline (Fig. 4D and E, blue traces). After isoflurane increase, we observe neither a detectable high frequency (Fig. 4D, red traces) nor low frequency response (Fig. 4E, red traces).

Notably, we found that the amplitude of the low and high pass voltage traces in response to the distensions was not uniform across all instances. This variation is attributed to the inherent variability in pressure applied due to slight variations in the placement of ligating sutures, etc. Given that the pressure levels were not identical, comparing response amplitudes directly should be avoided. Interestingly, our findings revealed instances where the initial peak in response was more pronounced, while in others, the secondary peak was larger (Fig. S5). This variability strongly suggests a significant blockage (‘silencing’), as quantified by the computation of the normalized Area Under the Curve (nAUC) for all low-frequency distension traces conducted before and after the application of isoflurane in all experiments (Fig. 4F).

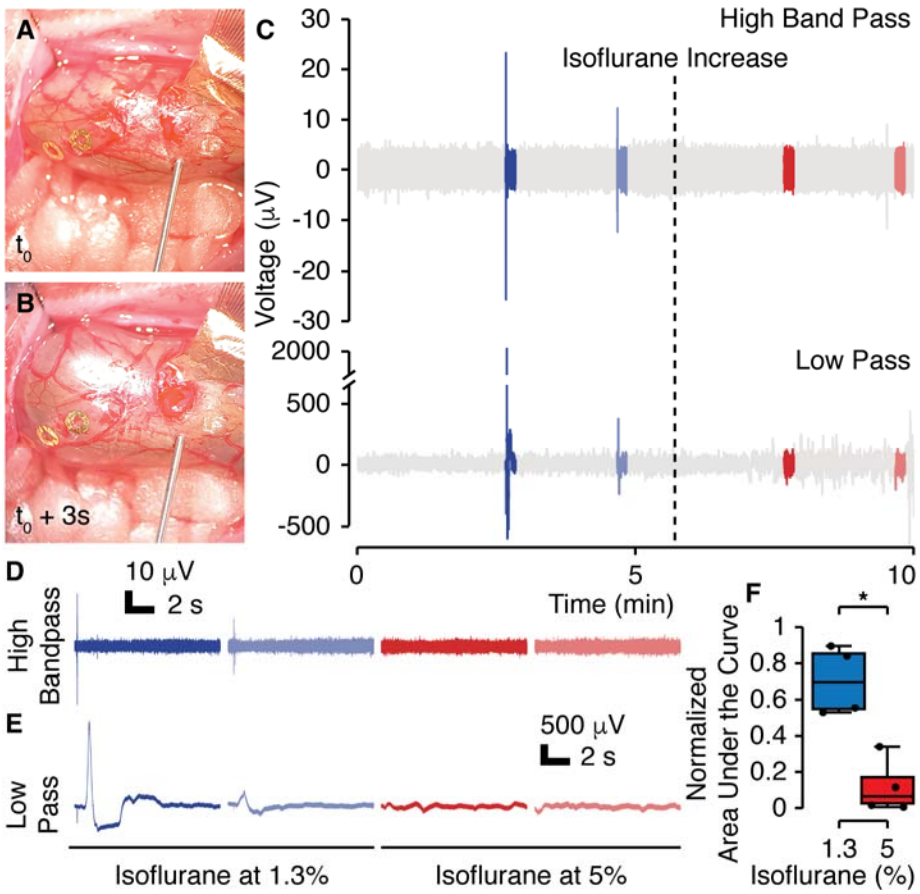

Fig. 4. Recording of Responses to Mechanical Stimuli. (**A**) Ligated portion of the colon with device implanted into the colonic wall prior to distension at t_0. (**B**) Distended colon during saline injection. (**C**) High-frequency bandpass (300 - 2000 Hz) and low pass (<300 Hz) representative full voltage traces. Segments highlighted in color represent 10 s intervals following each distension. Isoflurane was initially at 1.3% (blue) and was increased to 5% (red) at the time represented by the dashed line. (**D**) Zoom in on the high-frequency bandpass traces corresponding to the distension segments. (**E**) Zoom in on the low pass traces corresponding to the distension segments. (**F**) Normalized Area Under the Curve (nAUC) for all the low-frequency distension traces (10 s window) before and after the rise in isoflurane concentration (n = 4 rats, see Fig. S5 for traces from other animals). The nAUC standardizes the AUC obtained from each 10 s window by the range value within each experiment, ensuring a fair assessment of the responses across different animals. *: Statistically significant difference with $p<0.04$ using t-test after criteria for normality and variance homogeneity assumptions were met. The quantification of the nAUC for the high-frequency segments was not deemed meaningful due to the short duration of the response (<20 ms). To verify the biological origin of the recorded signals, we also conducted a thorough assessment of potential sources of interference by palpating the tissue and changing the electrical setup through movement of the ground on numerous animals to ensure that we did not misclassify mechanical artifacts as electrophysiological signal. These experiments, as well as the distension experiment under varying isoflurane concentrations confirmed that the signal is electrophysiological in origin.

This ‘silencing’ response due to increase of isoflurane may be explained by a direct reduction of neural activity (*25*, *26*) or by an anesthetic-induced muscle relaxation (*27*), leading to an elevated

threshold for eliciting a response. In other words, the muscle's state of relaxation under the influence of higher doses of isoflurane may require a higher stimulus or pressure to activate neural responses. Under this hypothesis, the isoflurane would not be silencing the neurons directly; instead, the muscle's increased relaxation would demand a greater level of stimulation to trigger a neural response. In either case, we can confirm the biological nature of the recorded signals, but the intricate interplay of the gastrointestinal components introduces a level of complexity that challenges the precise determination of their origin. We hypothesize that the interstitial cells of Cajal, crucial intermediates in the GI tract working as a bridge between neurons and muscle tissues, may have significantly contributed to the recorded activity following distension. These specialized cells are not only integral to the coordination of peristaltic movements but also exhibit electrophysiological activity themselves (*28*). To examine the specific effects of the anaesthetic, we also performed recordings using anaesthetic agents which are known to have limited neural suppression, i.e. urethane. We observed a more consistent response (Fig. S6), but we found that the typical route of application for urethane through an intraperitoneal injection was infeasible for repeat experiments, given the location of the colon within the peritoneal cavity.

Chronic Electrophysiology in Freely-moving Animals

To validate the capabilities of our devices for chronic electrophysiology, we used an exact mimic of the form factor we used for acute electrophysiology for comparative purposes in a chronic model, but with modified backend electronics (Fig. S7) to accommodate the substantial motion of the colon and surrounding tissues in the context of a freely-moving animal. This device was designed to be compatible with a percutaneous shoulder connector to access the implant (Fig. 5A, B) during a recording session, with the ground for the recording situated within the subcutaneous pocket adjacent to the percutaneous port (Fig. 5B). Using this design, we conducted open field recordings on three days over 2 weeks (days 1, 7, and 14), following the same methodology for each session. To standardize recording conditions, food was removed at 8 am on the day of recording, allowing for a minimum 4-hour period of food restriction. At noon, we initiated the recording by connecting the device to the acquisition system with the animals remaining in their cages to avoid restraining the animals leading to stress (Movie S4). After establishing a 30-minute baseline, a palatable food, Nutella® (3g), was left in the cage without disturbing the animals, and recordings continued for at least 1 additional hour. The animals underwent training prior to the surgery to consume Nutella® left in the cage, ensuring a consistent response to the stimulus.

The voltage traces in the high-frequency domain (300-4000 Hz) (Fig. 5C, D, and E) show consistencies in the amplitude across days prior to feeding. Some short high-amplitude variations in high-frequency voltage response can be seen in the pre-feeding traces, beginning on Day 7 (Fig. 5D), and becoming further defined by Day 14 (Fig. 5E). These changes are in accordance with the shift in impedance for the implant, which decrease from Day 1 to Day 7, before slightly increasing from Day 7 to Day 14 (Fig. 5F). This progression in impedance is consistent with responses observed in peripheral tissues, which typically have faster healing times than tissues of the central nervous system in the context of neural implant placement (*13*, *29*, *30*). Changes in metrics extracted from the recorded gut activity were identified at different times prior, during, and after feeding (Fig. S8). This suggests the potential for long-term monitoring and investigation of gastrointestinal dynamics in relation to feeding behavior or other external stimuli.

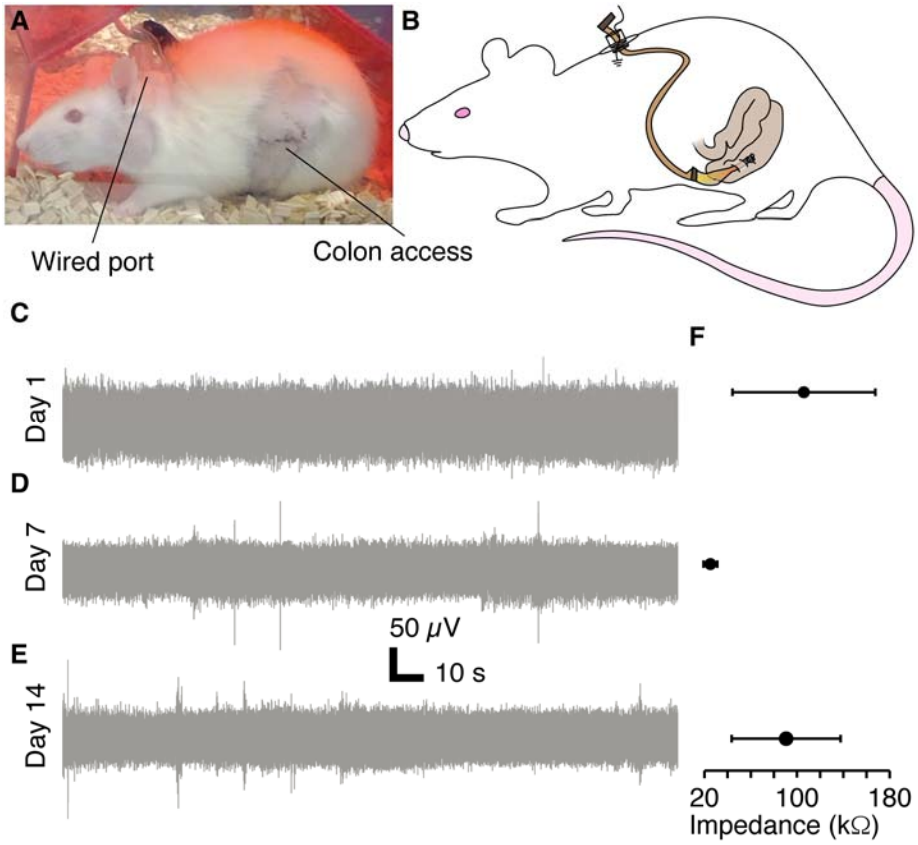

Fig. 5. Development of ENS recording system in freely-moving rodents. (**A**) Image showing rat with implanted device during recording. (**B**) Schematic detailing the placement of wiring and device within the animal. The wiring (Fig. S7) was routed subcutaneously between the percutaneous port down to the ventrolateral flank of the animal, where it crossed the peritoneal wall, allowing for implantation of the microfabricated portion of the device into the colon. Representative voltage traces from (**C**) Day 1, (**D**) Day 7, and (**E**) Day 14, filtered using a high band pass filter from 300 to 4000 Hz. (**F**) Mean impedance values for each day with standard deviation for same 5 channels across Days 1, 7, and 14.

We present a strategy and associated device for achieving neural recordings from the ENS in anaesthetized and freely-moving animals. Our data shows that rational design of bioelectronic devices coupled with surgical innovation allows access to traditionally difficult-to-reach areas of physiology. The ENS presents a particularly challenging region of the nervous system to access, given its inherent susceptibility to suppression from anaesthetic agents, its location within a highly mobile and elastic tissue, and its disperse and somewhat sparse distribution (ganglionated plexi of nerves) within the walls of the GI tract. Utilizing current methodologies for flexible device production, we were able to overcome these issues to record neural activity from the ENS. These studies set the groundwork for exploring an important and consequential region of the nervous system and lay the framework for the democratization of neural recording technologies to the vast areas of the body that are supported by the peripheral nervous system.

References

1. J. B. Furness, The enteric nervous system and neurogastroenterology. *Nat Rev Gastroenterol Hepatol* **9**, 286–294 (2012).

2. N. J. Spencer, H. Hu, Enteric nervous system: sensory transduction, neural circuits and gastrointestinal motility. *Nat Rev Gastroenterol Hepatol* **17**, 338–351 (2020).
3. D. Borgmann, E. Ciglieri, N. Biglari, C. Brandt, A. L. Cremer, H. Backes, M. Tittgemeyer, F. T. Wunderlich, J. C. Brüning, H. Fenselau, Gut-brain communication by distinct sensory neurons differently controls feeding and glucose metabolism. *Cell Metab* **33**, 1466-1482.e7 (2021).
4. J. F. Cryan, K. J. O'Riordan, C. S. M. Cowan, K. V. Sandhu, T. F. S. Bastiaanssen, M. Boehme, M. G. Codagnone, S. Cussotto, C. Fulling, A. V. Golubeva, K. E. Guzzetta, M. Jaggar, C. M. Long-Smith, J. M. Lyte, J. A. Martin, A. Molinero-Perez, G. Moloney, E. Morelli, E. Morillas, R. O'Connor, J. S. Cruz-Pereira, V. L. Peterson, K. Rea, N. L. Ritz, E. Sherwin, S. Spichak, E. M. Teichman, M. van de Wouw, A. P. Ventura-Silva, S. E. Wallace-Fitzsimons, N. Hyland, G. Clarke, T. G. Dinan, The Microbiota-Gut-Brain Axis. *Physiol Rev* **99**, 1877–2013 (2019).
5. T. R. Sampson, J. W. Debelius, T. Thron, S. Janssen, G. G. Shastri, Z. E. Ilhan, C. Challis, C. E. Schretter, S. Rocha, V. Gradinaru, M.-F. Chesselet, A. Keshavarzian, K. M. Shannon, R. Krajmalnik-Brown, P. Wittung-Stafshede, R. Knight, S. K. Mazmanian, Gut Microbiota Regulate Motor Deficits and Neuroinflammation in a Model of Parkinson's Disease. *Cell* **167**, 1469-1480.e12 (2016).
6. W. Morales-Soto, J. Gonzales, W. F. Jackson, B. D. Gulbransen, Enteric glia promote visceral hypersensitivity during inflammation through intercellular signaling with gut nociceptors. *Sci Signal* **16** (2023).
7. A. V. Zholos, D. O. Dryn, M. I. Melnyk, General anaesthesia-related complications of gut motility with a focus on cholinergic mechanisms, TRP channels and visceral pain. *Front Physiol* **14** (2023).
8. S. C. Pearce, H. G. Coia, J. P. Karl, I. G. Pantoja-Feliciano, N. C. Zachos, K. Racicot, Intestinal in vitro and ex vivo Models to Study Host-Microbiome Interactions and Acute Stressors. *Front Physiol* **9** (2018).
9. M. M. Buckley, D. O'Malley, Development of an ex Vivo Method for Multi-unit Recording of Microbiota-Colonic-Neural Signaling in Real Time. *Front Neurosci* **12** (2018).
10. S. Vignali, N. Peter, G. Ceyhan, I. E. Demir, F. Zeller, D. Senseman, K. Michel, M. Schemann, Recordings from human myenteric neurons using voltage-sensitive dyes. *J Neurosci Methods* **192**, 240–248 (2010).
11. C. Cirillo, J. Tack, P. Vanden Berghe, Nerve activity recordings in routine human intestinal biopsies. *Gut* **62**, 227–235 (2013).
12. A. E. Rochford, A. Carnicer-Lombarte, M. Kawan, A. Jin, S. Hilton, V. F. Curto, A. L. Rutz, T. Moreau, M. R. N. Kotter, G. G. Malliaras, D. G. Barone, Functional neurological restoration of amputated peripheral nerve using biohybrid regenerative bioelectronics. *Sci Adv* **9** (2023).
13. A. J. Boys, A. Carnicer□Lombarte, A. Güemes□Gonzalez, D. C. van Niekerk, S. Hilton, D. G. Barone, C. M. Proctor, R. M. Owens, G. G. Malliaras, 3D Bioelectronics with a Remodellable Matrix for Long□Term Tissue Integration and Recording. *Advanced Materials* **35** (2023).
14. A. Carnicer-Lombarte, A. J. Boys, A. Güemes, J. Gurke, S. Hilton, D. G. Barone, G. G. Malliaras, Ultraconformable cuff implants for long-term bidirectional interfacing of peripheral nerves at sub-1 nerve resolutions. doi: 10.1101/2023.04.14.536862.

15. A. Sahasrabudhe, L. E. Rupprecht, S. Orguc, T. Khudiyev, T. Tanaka, J. Sands, W. Zhu, A. Tabet, M. Manthey, H. Allen, G. Loke, M. J. Antonini, D. Rosenfeld, J. Park, I. C. Garwood, W. Yan, F. Niroui, Y. Fink, A. Chandrakasan, D. V. Bohórquez, P. Anikeeva, Multifunctional microelectronic fibers enable wireless modulation of gut and brain neural circuits. *Nat Biotechnol*, doi: 10.1038/s41587-023-01833-5 (2023).
16. D. Khodagholy, J. N. Gelinas, T. Thesen, W. Doyle, O. Devinsky, G. G. Malliaras, G. Buzsáki, NeuroGrid: recording action potentials from the surface of the brain. *Nat Neurosci* **18**, 310–315 (2015).
17. A. G. Polyravas, N. Schaefer, V. F. Curto, A. B. Calia, A. Guimera-Brunet, J. A. Garrido, G. G. Malliaras, Effect of channel thickness on noise in organic electrochemical transistors. *Appl Phys Lett* **117** (2020).
18. B. Liu, J. E. Linley, X. Du, X. Zhang, L. Ooi, H. Zhang, N. Gamper, The acute nociceptive signals induced by bradykinin in rat sensory neurons are mediated by inhibition of M-type K+ channels and activation of Ca2+-activated Cl– channels. *Journal of Clinical Investigation* **120**, 1240–1252 (2010).
19. M. Pasierski, B. Szulczyk, Beneficial Effects of Capsaicin in Disorders of the Central Nervous System. *Molecules* **27**, 2484 (2022).
20. A. Szallasi, D. N. Cortright, C. A. Blum, S. R. Eid, The vanilloid receptor TRPV1: 10 years from channel cloning to antagonist proof-of-concept. *Nat Rev Drug Discov* **6**, 357–372 (2007).
21. V. P. Zagorodnyuk, N. J. Spencer, Localization of the Sensory Neurons and Mechanoreceptors Required for Stretch-Evoked Colonic Migrating Motor Complexes in Mouse Colon. *Front Physiol* **2** (2011).
22. K. Matsumoto, T. Hosoya, K. Tashima, T. Namiki, T. Murayama, S. Horie, Distribution of transient receptor potential vanilloid 1 channel-expressing nerve fibers in mouse rectal and colonic enteric nervous system: relationship to peptidergic and nitrergic neurons. *Neuroscience* **172**, 518–534 (2011).
23. R. A. Roberts, W. J. Gullick, Bradykinin receptors undergo ligand-induced desensitization. *Biochemistry* **29**, 1975–1979 (1990).
24. J. B. Furness, M. Costa, Types of nerves in the enteric nervous system. *Neuroscience* **5**, 1–20 (1980).
25. H. A. Silverman, A. Stiegler, T. Tsaava, J. Newman, B. E. Steinberg, E. B. Masi, S. Robbiati, C. Bouton, P. T. Huerta, S. S. Chavan, K. J. Tracey, Standardization of methods to record Vagus nerve activity in mice. *Bioelectron Med* **4**, 3 (2018).
26. M. Nowicki, P. Baum, J. Kosacka, M. Stockinger, N. Klöting, M. Blüher, I. Bechmann, K. V. Toyka, Effects of isoflurane anesthesia on F□waves in the sciatic nerve of the adult rat. *Muscle Nerve* **50**, 257–261 (2014).
27. N. Kokita, T. A. Stekiel, M. Yamazaki, Z. J. Bosnjak, J. P. Kampine, W. J. Stekiel, Potassium Channel-mediated Hyperpolarization of Mesenteric Vascular Smooth Muscle by Isoflurane . *Anesthesiology* **90**, 779–788 (1999).
28. K. M. Sanders, S. D. Koh, S. M. Ward, Interstitial cells of cajal as pacemakers in the gastrointestinal tract. *Annu Rev Physiol* **68**, 307–343 (2006).
29. C. Metallo, R. D. White, B. A. Trimmer, Flexible parylene-based microelectrode arrays for high resolution EMG recordings in freely moving small animals. *J Neurosci Methods* **195**, 176–184 (2011).

30. D. Farina, K. Yoshida, T. Stieglitz, K. P. Koch, Multichannel thin-film electrode for intramuscular electromyographic recordings. *J Appl Physiol* **104**, 821–827 (2008).
31. N. D. Nagahawatte, N. Paskaranandavadivel, L. K. Cheng, "Characterization of Slow Wave Activity in Ex-vivo Porcine Small Intestine Segments" in *2021 43rd Annual International Conference of the IEEE Engineering in Medicine & Biology Society (EMBC)* (IEEE, 2021), pp. 7296–7299.
32. F. Crenner, F. Angel, C. Ringwald, Ag/AgCl electrode assembly for thin smooth muscle electromyography. *Med Biol Eng Comput* **27**, 346–356 (1989).
33. S. Middya, A. Carnicer□Lombarte, V. F. Curto, S. Hilton, A. Genewsky, A. L. Rutz, D. G. Barone, G. S. Kaminski Schierle, A. Sirota, G. G. Malliaras, Multishank Thin□Film Neural Probes and Implantation System for High□Resolution Neural Recording Applications. *Adv Electron Mater*, 220083 (2022).

Acknowledgments: The authors would like to acknowledge Alejandro Carnicer Lombarte for holding the animal license under which the study was conducted and his support in histological analysis, Tobias E. Naegele for his work on the design of the custom-made FFC and engineering the vascular connector, Chaeyeon Lee for supporting the histology analysis and animal work, Sam Hilton for supporting the animal work, and Sagnik Middya for his advice in backend electrical design and implementation. The authors would also like to acknowledge MRC Metabolic Diseases Unit (MC_UU_00014/5) for histological processing of paraffin-embedded sections. The views expressed are those of the author(s) and not necessarily those of the NIHR or the Department of Health and Social Care. For the purpose of open access, the authors have applied a Creative Commons Attribution (CC BY) license to any Author Accepted Manuscript version arising from this submission.

Funding:

HFSP Cross-disciplinary Fellowship [LT000034-C/2020] (AJB)

Royal Commission for the Exhibition of 1851 Research Fellowship (AGG).

NIHR Cambridge Biomedical Research Centre [NIHR203312] (GGM)

US Airforce Office of Scientific Research (AFOSR) [FA8655-20-1-7021] (RMO)

Science Foundation Ireland [12/RC/2273_P2] (NPH, FHU)

Marie Skłodowska-Curie Action COFUND Programme (APEX) [754535] (FHU)

Cambridge Trust Fellowship (RAG)

Author contributions:

Conceptualization: AJB, RMO

Methodology: AJB, AGG, RAG, FHU

Investigation: AJB, AGG, RAG

Formal analysis: AJB, AGG

Visualization: AJB, AGG

Code: AGG

Funding acquisition: AJB, DCB, GGM, RMO

Project administration: RMO

Supervision: NPH, DCB, GGM, RMO

Writing – original draft: AJB, AGG

Writing – review & editing: AJB, AGG, RAG, FHU, NPH, DCB, GGM, RMO

Competing interests: The authors declare no competing interests.

Data and materials availability: All data, code, and materials used in this analysis are listed in the main text or the supplementary materials, are available on request, or have been uploaded to a repository.

Supplementary Materials

Materials and Methods

Figs. S1 to S8

Movies S1 to S4